OPO OPHTHALMIC & PHYSIOLOGICAL OPTICS
THE JOURNAL OF THE COLLEGE OF OPTOMETRISTS

Ophthalmic & Physiological Optics ISSN 0275-5408

Zernike vs. Bessel circular functions in visual optics

Juan P Trevino[1], Jesus E Gómez-Correa[1], D Robert Iskander[2] and Sabino Chávez-Cerda[1]

[1]Departamento de Optica, Instituto Nacional de Astrofísica, Optica y Electrónica, Puebla, México, and [2]Institute of Biomedical Engineering and Instrumentation, Wroclaw University of Technology, Wroclaw, Poland

Citation information: Trevino JP, Gómez-Correa JE, Iskander DR & Chávez-Cerda S. Zernike vs. Bessel circular functions in visual optics. *Ophthalmic Physiol Opt* 2013, **33**, 394–402. doi: 10.1111/opo.12065

Keywords: bessel functions, corneal topography, deformable mirrors, influence functions, Sturm Liouville, Zernike polynomials

Correspondence: Juan P Treviño
E-mail address: trevinojp@inaoep.mx

Received: 1 November 2012; Accepted: 26 March 2013

Abstract

Purpose: We propose the Bessel Circular Functions as alternatives of the Zernike Circle Polynomials to represent relevant circular ophthalmic surfaces.
Methods: We assess the fitting capabilities of the orthogonal Bessel Circular Functions by comparing them to Zernike Circle Polynomials for approximating a variety of computationally generated surfaces which can represent ophthalmic surfaces.
Results: The Bessel Circular Functions showed better modelling capabilities for surfaces with abrupt variations such as the anterior eye surface at the limbus region, and influence functions. From our studies we find that the Bessel Circular Functions can be more suitable for studying particular features of post surgical corneal surfaces.
Conclusions: We show that given their boundary conditions and free oscillating properties, the Bessel Circular Functions are an alternative for representing specific wavefronts and can be better than the Zernike Circle Polynomials for some important cases of corneal surfaces, influence functions and the complete anterior corneal surface.

Introduction

In the field of vision and visual optics there is a number of surfaces related either to the anatomy and physiology of the eye or to optical instruments designed to measure and correct its aberrations. Some examples of real surfaces are the tear film and anterior corneal surfaces. On the other hand, there exist phase surfaces such as wavefronts and wavefront aberrations as well as influence functions in deformable mirrors. It is important to measure and mathematically model these surfaces in order to study their properties. There has been an extensive utilisation of Zernike Circle Polynomials (ZCP) to represent all of these surfaces regardless of their nature (real surfaces or phase functions). The ZCP are now the standard functions for the description of wave front aberrations of the human eye and have been also used in the modelling of corneal surfaces.[1–6] Although ZCP representation has proved to be useful in describing the majority of corneal surfaces, there are some reports showing their limitations, particularly when applied to complex ophthalmic surfaces with high spatial frequency content or 'discontinuities' resulting from surgical interventions.[6–11]

Many alternative functional representations have been proposed to describe ophthalmic surfaces, ranging from generalised conic functions to more complicated representations such as the fractional Zernike polynomials and spherical harmonics.[12–14] Other techniques include combinations of modal and zonal approaches.[15–17] Each of these approaches exhibits certain advantages and disadvantages with respect to the standard ZCP representation. As in the case of the ZCPs, none of them, however, is able to adequately account for a possible high spatial frequency content occurring in an ophthalmic surface, as it appears, for example, in total anterior eye surface including cornea, limbus, and sclera, or in higher ocular aberrations in the transitional zones of a progressive corrective lens.[18–20] It has been noted that the simple increase in the model order of the polynomial decompositions (i.e., over-parameterization) does not improve the representation of those surfaces.[4]

The origin of the ZCPs can be traced to a mathematical physics theory known as Sturm-Liouville (S-L) theory.[21,22]

Within the framework of this theory, the set of ZCPs is only a member of a class of families of functions that are orthogonal in the unit disk, meaning that a sum of them can be used to approximate any surface defined in that domain. The Bessel Circular Functions (BCF), which arise naturally in many two dimensional problems with cylindrical symmetry, is another example of the aforementioned class. This set of functions have been applied in different fields that range from modelling impact crater surface elevation to pattern recognition.[23,24] The BCF due to their more uniform and radial quasi-periodic behaviour have advantages over the ZCP when approximating surfaces with high frequency content.

We aim to investigate the applicability of BCF in modelling ophthalmic surfaces, applying a rigorous and systematic analysis and evaluating advantages and disadvantages of the BCF representation with respect to those of the ZCP.

Methods

Modal representation of surfaces

The Zernike Circular Polynomials (ZCP) were first obtained by Nijboer[25] by applying the S-L theory.[21,22] In general, this theory allows to construct complete and orthogonal sets of functions or modes. The ZCPs and the BCFs are both obtained from applying the S-L theory to a particular two variable rotationally invariant partial differential equation (RIPDE) with a different choice of parameters and boundary conditions. The corresponding solutions, ZCPs and BCFs are obtained as a separable product of an azimuthal and a radial function. For both sets, the azimuthal factor is given by

$$\begin{aligned} \phi_m &= \sin(m\varphi) \text{ for odd } m \\ \phi_m &= \cos(m\varphi) \text{ for even } m \end{aligned} \tag{1}$$

These functions can be also expressed in complex form, $\phi = \exp(\pm im\varphi)$. This representation should not be regarded merely as an alternative to the sine and cosine representation, since it has important physical interpretations. For instance, they are applied in the representation of complex pupils[26], the extended Nijboer-Zernike analysis[27], and Laguerre-Gaussian beam mode propagation[28]. For the ZCP, the most accepted representation of their radial function is[1]

$$R_n^{|m|}(r) = \sum_{s=0}^{(n-|m|)/2} \frac{(-1)^s (n-s)!}{s!\left(\frac{n+|m|}{2}-s\right)!\left(\frac{n-|m|}{2}-s\right)!} r^{n-2s} \tag{2}$$

where n $\geq$ m so the parity of a polynomial is the same as the corresponding *n*. Putting together the two variable modes in this case yields the ZCPs which are given in normalised form by:

$$Z_n^m(r,\varphi) = \sqrt{\frac{2(n+1)}{1+\delta_{m,0}}} R_n^m(r) {}^{\cos}_{\sin}(m\varphi). \tag{3}$$

The mathematical properties of the ZCPs have been extensively studied and widely discussed.[29,30] Each one of the Zernike modes is associated to a number known as eigenvalue, given by $\gamma = n(n+2)$ that appears in the RIPDE mentioned above, i.e. these eigenvalues arise from the S-L theory. These eigenvalues are used to determine an ordering scheme for the Zernike pyramid as described by Mahajan.[31]

By choosing a different set of parameters and boundary conditions in the RIPDE[21,22], the radial solution is no longer the radial Zernike polynomials but the Bessel functions of the first kind[32]

$$J_m(c_{mk}r) = \sum_{s=0}^{\infty} \frac{(-1)^s}{s!(m+s)!} \left(\frac{c_{mk}r}{2}\right)^{m+2s}. \tag{4}$$

Notice that the Bessel functions of the first kind are *power series with infinitely many terms* as opposed to the finite number of terms of the Zernike radial polynomials. They are oscillatory quasi-periodic and their envelope decay as $1/(cr)^{1/2}$ as the argument *cr* grows[32]. Comparative plots are shown in *Figure 1*. For this case, the two dimensional

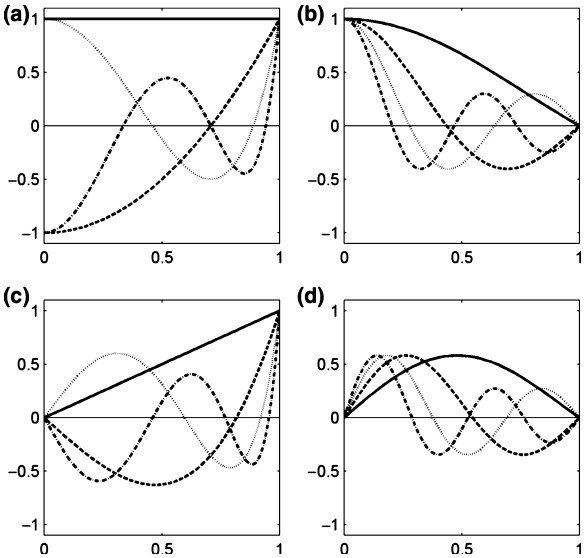

Figure 1. Radial Zernike Polinomials are plotted in a: m = 0, n =0, 2, 4, 6. c: m = 1, n =1, 3, 5, 7. Bessel functions of the first kind b: m = 0, n =1, 2, 3, 4. d: m = 1, n =1, 2, 3, 4. Although the radial order of the Bessel functions is lower, the number of intersections with the horizontal axis is the same.

modes are the BCFs which have a normalised expression given by

$$B_k^m(r,\varphi) = \sqrt{\frac{2}{1+\delta_{m,0}}}\frac{1}{J_{m+1}(c_{mk})}J_m(c_{mk}r)^{\cos}_{\sin}(m\varphi). \tag{5}$$

The corresponding eigenvalues γ of the BCFs are associated to the number k of zeros in the domain of the Bessel function J_m and is determined by $\gamma = c_{mk}$. This appear in the argument of the J_m, as a result, each function is scaled to its k-th zero. This scaling is related to the orthogonality of the Bessel functions.[32] As in the case of the ZCPs, the eigenvalues are used to establish the order for the BCFs.

The S-L theory establishes that an arbitrary function can be expanded as a linear combination of orthogonal modes:

$$S(\rho,\varphi) = \sum_{n,m}^{\infty} a_n^m \psi_n^m(\rho,\varphi), \tag{6}$$

where $\psi_n^m(\rho,\varphi)$, could be either ZCPs or BCFs, that are defined in the same domain as the function S. The coeffcients a_m^n are strength factors of the corresponding modes obtained from a superposition integral

$$a_n^m = \frac{1}{\pi}\int_0^1 \int_0^{2\pi} S(\rho,\varphi)\psi_n^m(\rho,\varphi)\rho d\rho d\varphi. \tag{7}$$

The ZCPs and BCFs are said to be complete orthogonal sets. Orthogonality of modes means in a broad sense, that in the modal expansion of the function $S(\rho, \varphi)$ each mode carries a certain amount of information about S which does not overlap the information carried by any of the other modes. Completeness, on the other hand, means that an arbitrary function like $S(\rho, \varphi)$ does not carry more information than the whole set of modes, so that the *complete* set of modes is capable of representing the surface. These two properties guarantee that any arbitrary function can be approximated as much as needed by its infinite modal expansion as expressed in equation (6) and will be equal if they satisfy the same boundary conditions.

Representing surfaces with finite models

As mentioned earlier, a finite model of a surface is always necessary for computational purposes. This means that the surface of interest will be sampled over the domain. This is noticeable, for example in Placido disk devices, where the corneal height data is represented by a cloud of discrete points. The number of functions employed for the modal expansion of the surface has to be finite also, so the infinite sum (6) is truncated to a finite number of terms. This truncated sum of modes is no longer equal to the function S, so an approximation error or fitting error has to be evaluated. Using a finite subset of orthogonal ZCP or BCF discrete (sampled) functions, we can form the linear model

$$S(\rho_d,\varphi_d) = \sum_{p=1}^{P} a_p\psi_p(\rho_d,\varphi_d) + \varepsilon_p(\rho_d,\varphi_d). \tag{8}$$

The subindex d refers to the sample point and the total number of samples is D. The single index p accounts for n, m indices used before. Equation (8) can be written in vector form as

$$S = \psi a + \varepsilon \tag{9}$$

where S is a column vector of D elements that represents a surface sampled at discrete points (ρ_d, φ_d), $d = 1, 2 \ldots D$. ψ is a ($D \times P$) matrix of orthogonal modes also sampled at discrete points: $\psi_p(\rho_d,\varphi_d)$. The vector a is a P -element column vector of coefficients, and ε is a column vector of D elements that represents the measurement and modelling error at the sample points. One is interested in finding the vector $\hat{a}$ of coefficient that minimises the square of this error. This is achieved by the least-squares method which yields

$$\hat{a} = (\psi^T\psi)^{-1}\psi^T S \tag{10}$$

where the superindex T denotes the transposition, provided that the inverse exists. We use this method to study how the BCF behave as compared to the standard ZCP in modelling ophthalmic surfaces.

Next we need to decide the finite subset of BCFs and ZCPs that will be compared. A reasonable requirement is that we use the same number of modes from each set. If we choose to organise the Bessel modes in terms of their associated eigenvalues, the arrangement results in an inverted pyramid (see *Figure 2*). This way, fixing the radial index for both sets will result in including modes with different azimuthal order and vice versa. However, we will have almost the same amount of modes in each base. The eigenvalues of the BCFs can be easily obtained numerically due to the quasi-periodic behaviour of the Bessel functions but are also widely available in tables[33] (Algorithms for finding successive zeros of Bessel functions are available at *MathWorks website*. The corresponding author has a custom tailored algorithm which he is willing to share).[33] So, it is easy to organise the BCF modes. We use the arrangement mentioned above to choose the set of BCFs that will be compared to the ZCPs. We have tested the Bessel functions as compared to the Zernike functions for a variety of artificially created surfaces. All the surfaces have been produced in a unit disk simulating a normalized pupil or corneal area.

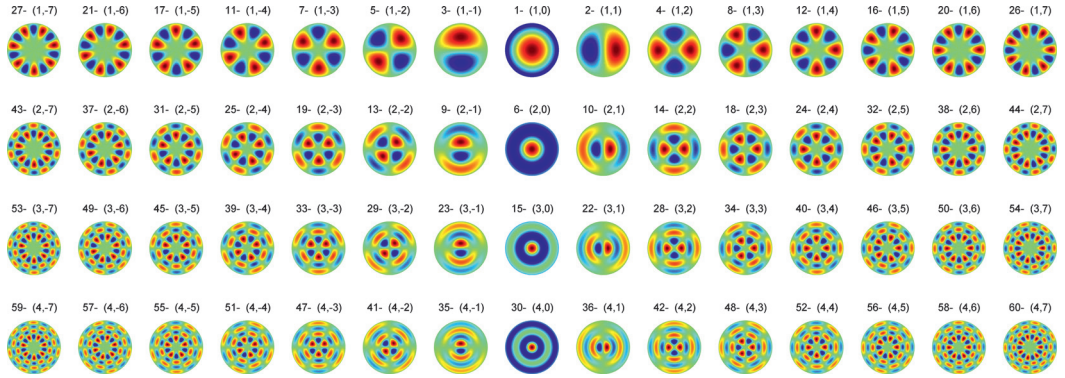

n \ m	−9	−8	−7	−6	−5	−4	−3	−2	−1	0	1	2	3	4	5	6	7	8	9
1			***7*** 27	***6*** 21	***5*** 17	***4*** 11	***3*** 7	***2*** 5	***1*** 3	***0*** 1	***1*** 2	***2*** 4	***3*** 8	***4*** 12	***5*** 16	***6*** 20	***7*** 26		
2			43	9 37	8 31	***6*** 25	***5*** 19	***4*** 13	***3*** 9	***2*** 6	***3*** 10	***4*** 14	***5*** 18	***6*** 24	8 32	9 38	44		
3			53	49	45	9 39	8 33	***7*** 29	***6*** 23	***4*** 15	***6*** 22	***7*** 28	8 34	9 40	46	50	54		
4			59	57	55	51	47	41	8 35	***7*** 30	8 36	42	48	52	56	58	60		

Figure 2. Graphical representation of the BCFs. The numbering is done according to the eigenvalues of the SL problem. The regions enclosed (inverted pyramids) can be used for benchmarking the BCF representation with the corresponding ZCP representation for different radialor azimuthal order. We used the first 30 terms enclosed in black.

Results

In order to compare the BCF base to the ZCP base a set of 30 BCFs was used, this subset included two modes for each of the orders m = 5,6,7 (see *Figure 2*). For the ZCPs, a number of 36 modes corresponding to n = 7 were employed. This choice was done fixing the azimuthal order, which yields a BCF radial order of n = 4.

A. Gaussian Surfaces

We started with an off axis Gaussian surface defined by

$$G(x,y) = A\exp\left\{\frac{(x-h)^2+(y-k)^2}{W^2}\right\} \qquad (11)$$

varying its width and the position of its centre. This type of function has been frequently used in the modelling of influence functions of adaptive optics systems.[34,35] A thin Gaussian i.e. $W^2 = 0.1$ would correspond to a flexible mirror, while a broader one, to a stiffer mirror. This type of function could also be useful to model Keratoconic corneas, since there is a protuberance on their anterior surface.

On axis Gaussian functions were better fitted by BCFs as long as the width was smaller than unity, the ZCP fitting becomes better at around $W^2 = 1.1$ which corresponds to a normalised surface with boundary condition of approximately 0.5. In *Figure 3* we present a set of three Gaussian surfaces with various widths at the same off axis position within the unit disk. The error figures display the rms error measured in dB units for increasing concentric subdomains. The figure shows a better fitting of the BCFs for off axis Gaussian functions of intermediate width. The behaviour inverts as the Gaussian function gets wider, the ZCPs give a better fitting in this case because the surface gets flatter. This effect is due to the higher radial frequencies of the BCFs and their zero boundary conditions. This same property of the BCFs causes larger modelling errors either when the Gaussian is broader than the unit disk or its centre is such that the surface is not fixed at the boundary of the unit disk.

In deformable mirrors, increasing the effective pupil of the system is equivalent to having narrower influence functions in the normalized domain. Since BCFs produce better fittings than ZCPs for narrower Gaussian surfaces, sufficiently close to the centre of the unit disk, they might help to control adaptive optics systems with larger effective pupils.

Surfaces with rings

A ring structure can be obtained by a radial Gaussian function centred at a radius r_0 and a constant angular factor,

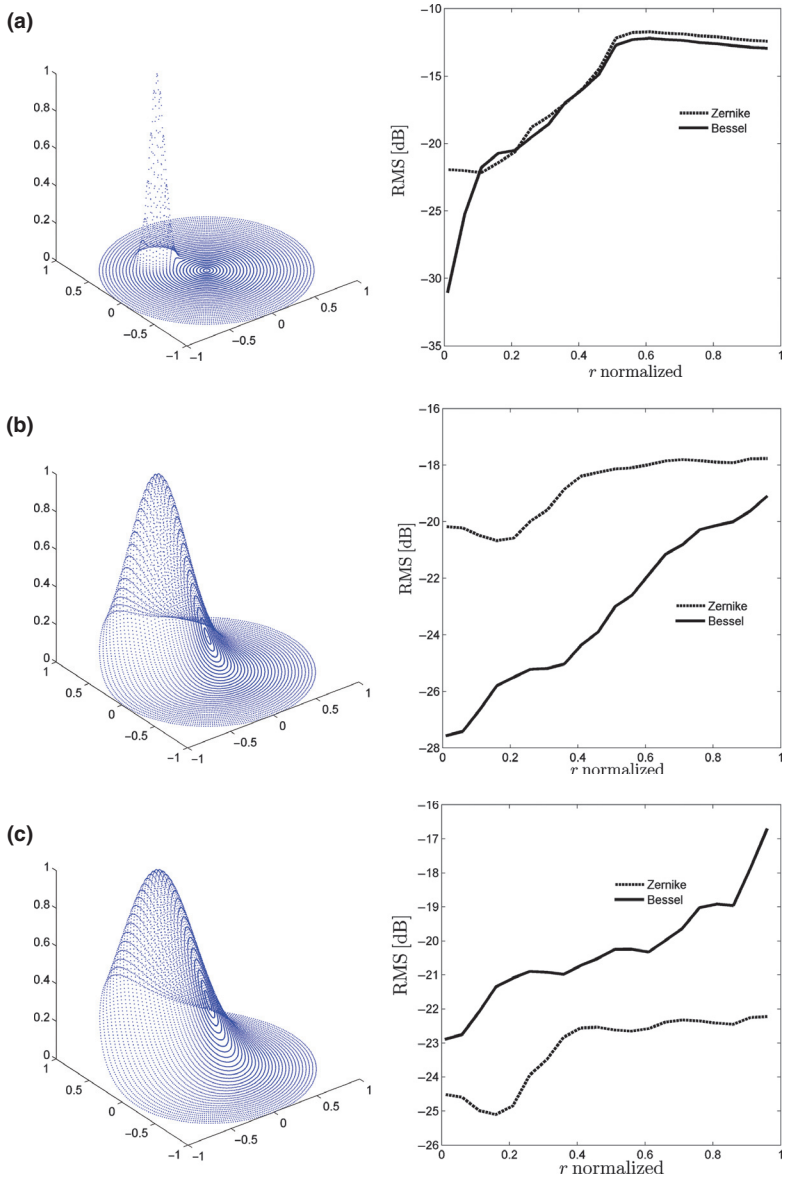

Figure 3. Gaussian functions of various widths a. w^2 =0.1 B. w^2 =0.5 and c. w^2 = 15 on a disk of r = 4. The BCFs approximate better for narrower Gaussian functions, while the ZCPs for wider ones. The zero boundary condition is also important for BCFs performance.

$$u(r,\varphi) = \exp\left\{\frac{-(r-r_0)^2}{W^2}\right\}. \qquad (12)$$

This type of surface could represent the effects of wearing a certain type of contact lenses. A multiple ringed surface, for instance a sum of two or more similar functions, could also represent a wavefront generated by a multifocal lens. We performed the comparison of BCFs and ZCPs with the same number of modes as in the previous case. Here, the BCFs presented a slightly better fitting capability for complete rings, especially at the central zone of the structure (*Figure 4*). If the ring structure is such that the boundary is not fixed at zero, the BCFs present a large fitting error. We also produced incomplete rings (*Figure 4*) by combining a radial Gaussian function with an azimuthal super-Gaussian function:

$$u(r,\varphi) = \exp\left\{\frac{-(r-r_0)^2}{W^2}\right\}\exp\left\{\frac{-(\varphi-\varphi_0)^{2N}}{W_\varphi^{2N}}\right\} \qquad (13)$$

where N is a positive integer. The fitting capabilities of the ZCPs and BCFs showed a very similar behaviour as that for

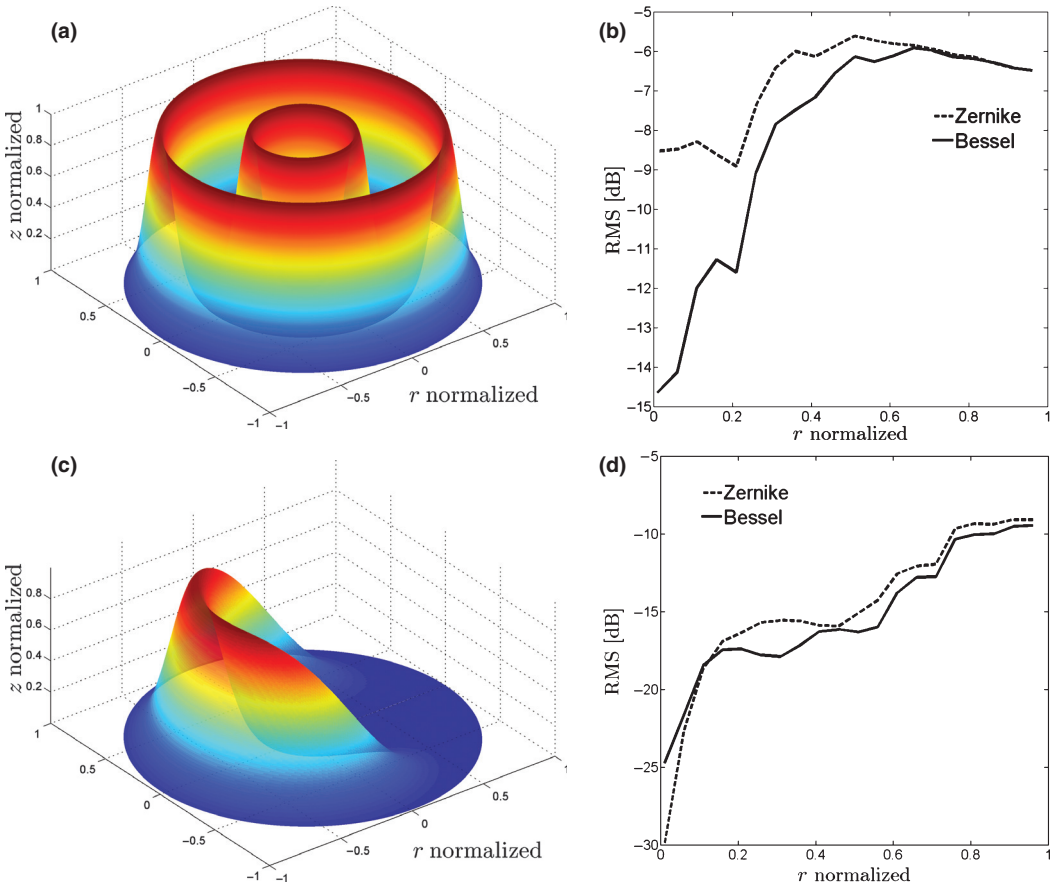

Figure 4. Gaussian rings are better approximated by the BCFs at the central region, but the errors converge. In the case of incomplete rings both sets produce very similar fitting errors.

complete rings, however if the incomplete ring structure gets closer to the centre, the BCFs produce a better fitting.

In real cases, concentric rings might be off axis, this fact will affect the fitting abilities of the BCFs, however a pre-processing of the data points would allow to re-centre the surface and perform the desired fitting. Incomplete ring structures could be useful in modelling the effect of the eye-lid pressure on the anterior corneal surface.

Some zonal approaches develop modal approximations at subsets of the corneal surface. Once the best sphere is subtracted from the main surface in this zone, the reminder is modelled. A rough model of a post-surgical surface, could be done in a semi meridian by:

$$u(r) = r^n \exp\left\{-\left(\frac{r}{W}\right)^2\right\}, \qquad (14)$$

Where n is a positive integer and W is a shape parameter. This surface exhibits a similar feature as the BCFs of $n \geq 1$ at the central zone. For this reason, the BCFs have a significantly better approximating performance for m = 5,6,7. We performed simulations for several values of W and n and in all cases the behaviour was similar to the one shown in *Figure 5*.

Complete eye model

An interesting case is the model of the total anterior eye surface, which includes the anterior surface of the cornea, limbus and sclera. This was done by etching together two spherical surfaces of different radii. To produce this model we employed typical parameters for anterior corneal radius, visible iris and diameter of the eye. This results in a surface with a discontinuity in the first derivative precisely in the limbus region (*Figure 6a* and its normalization b). The surface is radially symmetric, therefore we could choose modes of higher radial orders but restrict the set to $m = 0$. In *Figure 6c*, we present the approximating errors using only four modes of each base with $m = 0$. In this case it is not possible to decide which base is better. However, if we use five modes, the BCFs give a more stable error at the limbus region at $r = 0.6$, where the error increases in both cases

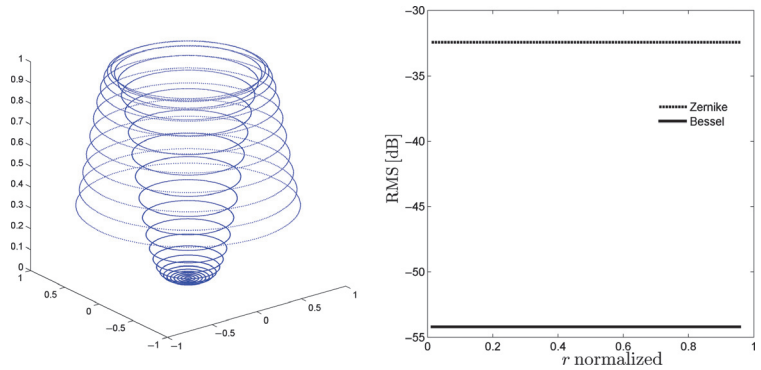

Figure 5. A post surgical surface, modelled by equation (14).The plot shows a significantly better fitting capability of the BCFs in this kind of surfaces.

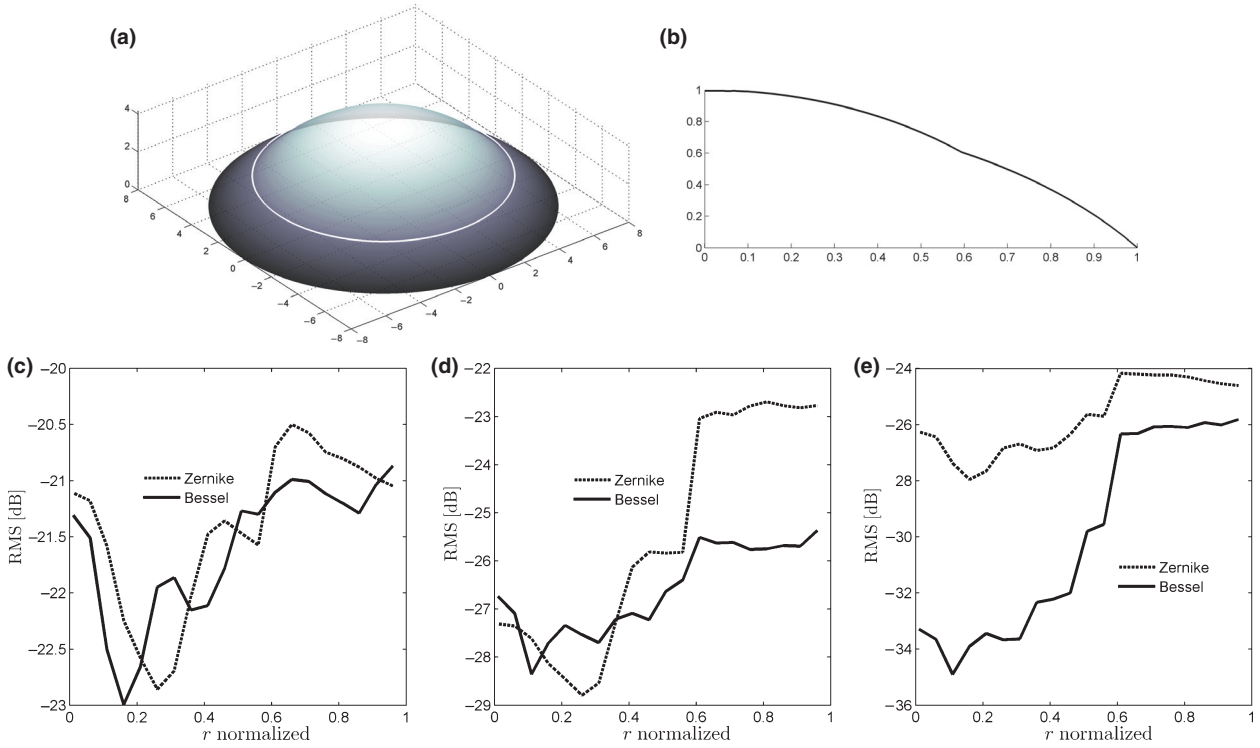

Figure 6. a. Total eye model with typical parameters. b. The normalised model. c. Fitting errors for four modes. d. Fitting error for five modes. E. Fitting error for six modes.

(see *Figure 6d*). In average, the error is smaller for the BCFs. If we increase the number of modes to six, the BCFs outperform the ZCPs in the whole surface and the fitting error remains smaller for the BCFs, as can be clearly seen in *Figure 6e*.

The BCFs have a better performance than the ZCPs when fitting this type of surfaces due to the fact that the radial component of the BCFs has more zeros, resulting in more oscillations, within the unit interval than the ZCPs for the same radial order.

Discussion

We can observe from *Figure 2* that some elements of the BCF base are similar to particular elements of the ZCP base making possible a rough analogy between the sets. An ordering of the BCFs according to the eigenvalues of the equation leads to a matching mode scheme which makes sense in terms of the aforementioned analogy. Once the number of modes is fixed, the BCFs show a very good behaviour for centred structures such as Gaussian

functions, and surfaces with many radial ripples. However the approximating error for BCFs increases for surfaces with considerable amplitude at the boundary of the circular domain because of the required zero boundary condition of the BCF set. The very smooth surfaces were better represented by the ZCPs because the quadratic nature of the low order terms carry enough information to describe such surfaces.

A given value of the azimuthal order m restricts the corresponding elements of radial order n in the ZCP set. This does not happen in the BCF base, where there exist a mode for any combination or radial and azimuthal order. This gives the BCFs an advantage for representing surfaces of radial symmetry even when there are discontinuities in the first derivative, as in the model of the total anterior eye surface.

In most of the simulations in this work we restricted the BCFs to a set that exhibits similar features as the ZCPs and therefore limited their behaviour. However, we showed that the particular case of the total eye, by lifting this restriction and increasing the number of BCF modes with $m = 0$ resulted in a better performance.

Conclusions

We have presented the Bessel Circular Functions that are also orthogonal in the unit circle and compare them to the known Zernike Circular Polynomials to fit various surfaces which represent common cases appearing in the field of visual optics. We found out that the BCFs had a very good behaviour proving to be a competitive candidate for the ZCPs to represent all kinds of surfaces from front corneal surfaces to influence functions. The BCFs showed a better behaviour to model surfaces that present an abrupt variation as in the case of the total anterior eye surface at the limbus region, and influence functions. We also show that the BCF set is a suitable candidate to study particular features of post surgical corneal surfaces such as single ring surfaces resembling residual surfaces from ablations. A more detailed study of these cases will be published elsewhere. We expect to apply the BCFs to model influence functions on deformable mirrors in order to maximise the effective pupil. This set is a good candidate for modal expansion especially in complex pupil functions as approached by the Extended Zernike-Nijboer theory.

Acknowledgements

This research has been partially funded by Consejo Nacional de Ciencia y Tecnología (CONACYT) and Endeavour Awards (Endeavour Research Fellowship 1703). We would like to thank the referees for valuable suggestions to improve the present manuscript. We would also like to thank Fan Yi from the CLVOL at QUT for valuable input for the present work.

References

1. American National Standards Institute. *Methods for reporting the optical aberrations of eyes*. American National Standards for Ophthalmics, ANSI Z80.28, 2004.
2. Schwiegerling J, Greivenkamp JE & Miller JM. Representation of videokeratoscopic height data with Zernike polynomials. *J Opt Soc Am (A)* 1995; 12: 2105–2113.
3. Schweigerling J & Greivenkamp JE. Using corneal height maps and polynomial decomposition to determine corneal aberrations. *Optom Vis Sci* 1997; 74: 906–916.
4. Iskander DR, Collins MJ & Davis B. Optimal modeling of corneal surfaces with zernike polynomials. *IEEE Trans Biomed Eng* 2001; 48: 87–95.
5. Iskander DR, Morelande MR, Collins MJ & Buehren T. A refined bootstrap method for estimating the zernike polynomial model order for corneal surfaces. *IEEE Trans Biomed Eng* 2004; 51: 2203–2206.
6. Klyce SD, Karon MD & Smolek MK. Advantages and disadvantages of the zernike expansion for representing wave aberration of the normal and aberrated eye. *J Refract Surg* 2004; 20: S537–S541.
7. Smolek MK & Klyce SD. Zernike polynomial fitting fails to represent all visually significant corneal aberrations. *Invest Ophthalmol Vis Sci* 2003; 44: 4676–4681.
8. Carvalho L A. Accuracy of zernike polynomials in characterizing optical aberrations and the corneal surface of the eye. *Invest Ophthalmol Vis Sci* 2005; 46: 1915–1926.
9. Wang L, Chernyak D, Yeh D & Koch D. Fitting behaviors of Fourier transform and Zernike polynomials. *J Cataract Refract Surg* 2007; 33: 999–1004.
10. Yoon G, Pantanelli S & MacRae S. Comparison of Zernike and Fourier wavefront reconstruction algorithms in representing corneal aberration of normal and abnormal eyes. *J Refract Surg* 2008; 24: 582–590.
11. Martínez-Finkelshtein A, Delgado AM, Castro GM, Zarzo A & Alió JL. Comparative analysis of some modal reconstruction methods of the shape of the cornea from the corneal elevation data. *Invest Ophthalmol Vis Sci* 2009; 50: 5639–5645.
12. Kasprzak HT & Iskander DR. Approximating ocular surfaces by generalised conic curves. *Ophthal Physiol Opt* 2006; 26: 602–609.
13. Schneider M, Iskander DR & Collins MJ. Modeling of corneal surfaces with rational functions for high speed videokeratoscopy data compression. *IEEE Trans Biomedical Eng* 2009; 56: 493–499.
14. Iskander DR. Modeling videokeratoscopic height data with spherical harmonics. *Optom Vis Sci* 2009; 86: 542–547.
15. Espinosa J, Mas D, Pérez J & Illueca C. Optical surface reconstruction technique through combination of zonal and modal fitting. *J Biomed Opt* 2010; 15: 026022.

16. Martínez-Finkelshtein A, Ramoz-López D, Castro-Luna GM & Alió JL. *An adaptive algorithm for the cornea modeling from keratometric data*. arXiv:1009:1244v1 [physics.medph], 2010.
17. González L, Hernández Matamoros J L & Navarro R. Multizone model for postsurgical corneas: analysis for standard and custom lasik outcomes. *J Biomed Opt* 2008; 13: 044035.
18. Jongsma FH, de Brabander J, Hendrikse F & Stultiens BA. Development of a wide field height eye topographer: validation on models of the anterior eye surface. *Optom Vis Sci* 1998; 75: 69–77.
19. Blendowske R, Villegas EA & Artal P. An analytical model describing aberrations in the progression corridor of progressive addition lenses. *Optom Vis Sci* 2006; 83: 666–671.
20. Raasch TW, Su L & Yi A. Whole-surface characterization of progressive addition lenses. *Optom Vis Sci* 2011; 88: E217–E226.
21. Gwaiz A M. *Sturm-Liouville Theory and its Applications*. Springer-Verlag: London, 2007.
22. Davis H F. *Fourier Series and Orthogonal Functions*. 2nd edition, Dover Publications Inc: NY, USA, 1989.
23. Wallis D. & Macbride N. Planetary impact crater analysis with eigenfunction expansion. *Mon Not R Astron Soc* 2002; 330: 458–472.
24. Wang Q, Ronneberger O & Burkhardt H. Rotational invariance based on fourier analysis in polar and spherical coordinates. *IEEE Trans Pattern Anal Mach Intell* 2009; 31: 1715–1722.
25. Nijboer BRA. *The diffraction theory of aberrations*. PhD thesis, University of Groningen: Groningen, 1942.
26. Navarro R, Rivera R & Aporta J. Representation of wavefronts in free-form transmission pupils with complex Zernike polynomials. *J Optom* 2011; 4: 41–48.
27. Braat JJM, Dirksen P & Janssen AJEM. Assessment of an extended Nijboer-Zernike approach for the computation of optical point-spread functions. *J Opt Soc Am (A)* 2002; 19: 858–870.
28. Trappe N, Murphy JA & Withington S. The gaussian beam mode analysis of classical phase aberrations in diffraction-limited optical systems. *Eur J Phys* 2003; 24: 403.
29. Born M & Wolf E. *Principles of Optics*. 7th (expanded) edition, Cambridge University Press: Cambridge, UK, 1999.
30. Mahajan V. *Optical Imaging and Aberrations Part I*. SPIE Optical Engineering Press: Bellingham, WA, 1998.
31. Mahajan V. *Aberration Theory Made Simple*. SPIE Optical Engineering Press: Bellingham, WA, 1991.
32. Bowman F. *Introduction to Bessel Functions*. Dover Publications Inc: NY, USA, 1958.
33. Beattie CI. Table of first 700 zeros of Bessel functions. *Bell Syst Tech J* 1958; 37: 689–697.
34. Huang L, Rao C & Jiang W. Modified Gaussian influence function of deformable mirror actuators. *Opt Express* 2008; 16: 108–114.
35. Roopashree MB, Akondy V & Prasad BR. A novel model of influence function: calibration of a continuous membrane deformable mirror. *ACEEE Int J on Control Systems and Instrumentation* 2012; 3: 10–14.